EBioMedicine 10 (2016) 124–136

Contents lists available at ScienceDirect

EBioMedicine

journal homepage: www.ebiomedicine.com

Research Paper

Dual Targeting of 3-Hydroxy-3-methylglutaryl Coenzyme A Reductase and Histone Deacetylase as a Therapy for Colorectal Cancer☆

Tzu-Tang Wei [a], Yi-Ting Lin [a], Wen-Shu Chen [a], Ping Luo [a], Yu-Chin Lin [a,e,h], Chia-Tung Shun [b,c], Yi-Hsin Lin [a], Jhih-Bin Chen [a,g], Nai-Wei Chen [g], Jim-Min Fang [g], Ming-Shiang Wu [d], Kai-Chien Yang [a], Li-Chun Chang [d], Kang-Yu Tai [i], Jin-Tung Liang [f], Ching-Chow Chen [a,*]

[a] Department of Pharmacology, National Taiwan University College of Medicine, Taipei 100, Taiwan
[b] Graduate Institute of Forensic Medicine, National Taiwan University College of Medicine, Taipei 100, Taiwan
[c] Department of Pathology, National Taiwan University Hospital, Taipei 106, Taiwan
[d] Division of Gastroenterology, Department of Internal Medicine, National Taiwan University Hospital, Taipei 106, Taiwan
[e] Department of Oncology, National Taiwan University Hospital, Taipei 106, Taiwan
[f] Department of Surgery, National Taiwan University Hospital, Taipei 106, Taiwan
[g] Department of Chemistry, National Taiwan University, Taipei 106, Taiwan
[h] Department of Internal Medicine, Far-Eastern Memorial Hospital, New Taipei City 220, Taiwan
[i] Genome and Systems Biology Degree Program, National Taiwan University, Academia Sinica, Taiwan

ARTICLE INFO

Article history:
Received 30 May 2016
Received in revised form 8 July 2016
Accepted 15 July 2016
Available online 17 July 2016

Keywords:
Colorectal cancer
HMG-CoA reductase
Histone deacetylase
Statin hydroxamate
Preclinical model

ABSTRACT

Statins are 3-hydroxy-3-methylglutaryl coenzyme A (HMG-CoA) reductase (HMGR) inhibitors decreasing serum cholesterol and have shown promise in cancer prevention. In this study, we demonstrated the oncogenic role of HMGR in colorectal cancer (CRC) by disclosing increased HMGR activity in CRC patients and its enhancement of anti-apoptosis and stemness. Our previous studies showed that statins containing carboxylic acid chains possessed activity against histone deacetylases (HDACs), and strengthened their anti-HDAC activity through designing HMGR-HDAC dual inhibitors, JMF compounds. These compounds exerted anti-cancer effect in CRC cells as well as in AOM-DSS and $Apc^{Min/+}$ CRC mouse models. JMF mostly regulated the genes related to apoptosis and inflammation through genome-wide ChIP-on-chip analysis, and Ingenuity Pathways Analysis (IPA) predicted their respective regulation by NR3C1 and NF-κB. Furthermore, JMF inhibited metastasis, angiogenesis and cancer stemness, and potentiated the effect of oxaliplatin in CRC mouse models. Dual HMGR-HDAC inhibitor could be a potential treatment for CRC.

1. Introduction

3-Hydroxy-3-methylglutaryl coenzyme A (HMG-CoA) reductase (HMGR) is the rate-limiting enzyme for cholesterol synthesis in the conversion of HMG-CoA to mevalonate. Statins are HMGR inhibitors decreasing serum cholesterol to reduce the incidence of cardiovascular and cerebrovascular disorders (Minder et al., 2012). In addition to cholesterol synthesis, activation of HMGR facilitated protein prenylation, such as farnesylation of Ras oncoproteins for cell growth and carcinogenesis (Thurnher et al., 2012). The mevalonate pathway was up-regulated by mutant p53 or activation of oncogenic signaling, such as HIF-1 or PI3K-Akt (Freed-Pastor et al., 2012; Semenza, 2003; Yuan and Cantley, 2008). Clinical studies also showed the promise of statins in cancer prevention (Simon et al., 2012; Poynter et al., 2005). Therefore, targeting HMGR-mevalonate pathway might be a strategy against cancer. However, the role of HMGR as an oncotarget remains to be elucidated.

Our previous studies demonstrated that statins containing carboxylic acid chains also had activity against histone deacetylase (HDAC), an important oncoprotein, to exert anti-cancer effects. Thus, statins may suppress tumor formation through the inhibition of both HMGR and HDAC activity (Lin et al., 2008). To further improve statins' activity against HDAC, three statin hydroxamates named compound 12, 13, and 14 as respective JMF3086, 3171, and 3173 were designed to inhibit class I and II HDACs and HMGR (Chen et al., 2013), and their anti-cancer activities were explored. Recently, the strategy of developing polypharmacological molecules that dually inhibit HDACs and other therapeutic targets has been reported (Falkenberg and Johnstone, 2014). Accordingly, whether dual targeting HMGR and HDAC is a strategy for treating cancer deserves further investigation.

Colorectal cancer (CRC) is a worldwide cancer with a rising annual incidence, leading to a significant mortality due to metastasis.

☆ Disclosures: The authors disclose no conflicts of interest.

* Corresponding author at: Department of Pharmacology, College of Medicine, National Taiwan University, No.1, Jen-Ai Road, 1st Section, Taipei 10018, Taiwan.
E-mail address: chingchowchen@ntu.edu.tw (C.-C. Chen).

http://dx.doi.org/10.1016/j.ebiom.2016.07.019

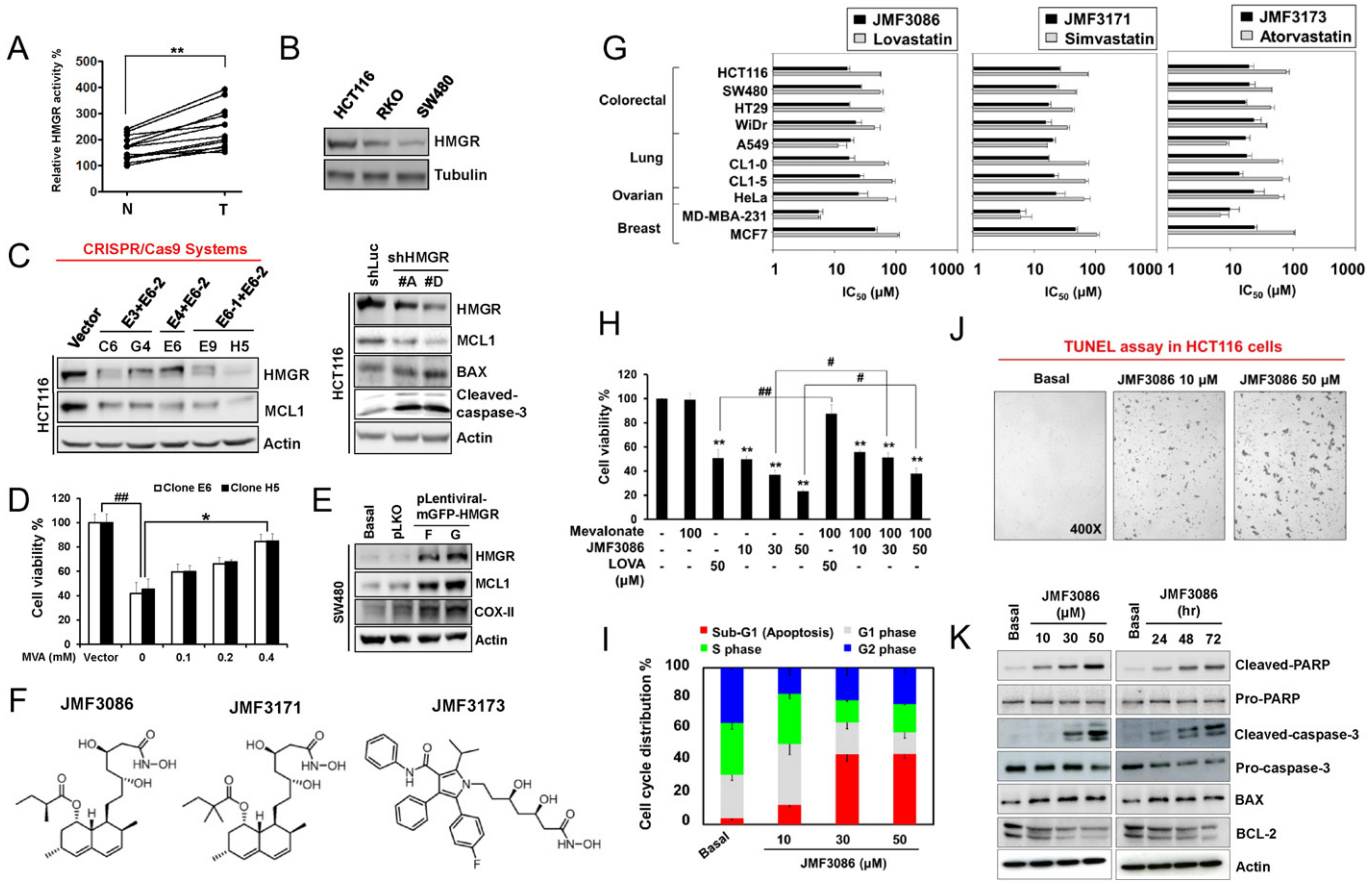

Fig. 1. Targeting HMG-CoA reductase in colorectal cancer cells and the effect of JMF compounds on cell viability and apoptosis. (A) HMGR activity in CRC tissues from patients (T) normalized to adjacent normal epithelium (N) is shown. The HMG-CoA reductase activity was measured according to NADPH oxidation by HMGR in the presence of the substrate HMG-CoA using an assay kit (CS-1090). 100 μg protein of tissue was mixed with NADPH and HMG-CoA (substrate), and incubated at 37 °C for 5 min. The absorbance at 340 nm was measured, and the decrease in A_{340} absorbance represented the oxidation of NADPH by the catalytic subunit of HMGR in the presence of the substrate HMG-CoA. The SPSS program (SPSS Inc.) was used for all statistical analysis, which was performed by two-sided Student's *t*-test. $^{**}P < 0.01$. (B) Western blot analysis for HMGR expression in CRC cells. (C) Effect of HMGR knockout on MCL1 expression in HCT116 cells by CRISPR technology (left panel). Effect of HMGR knockdown on MCL1, BAX and cleaved-caspase-3 expressions in HCT116 cells by shHMGR transfection (right panel). The suspension and attached cells were harvested. (D) HMGR-knockout stable clones were treated with different doses of mevalonate for 5 days and the cell viability was analyzed by MTT assay. $^{\#\#}P < 0.01$ versus vector; $^{*}P < 0.01$ versus 0 mM mevalonate. (E) Effect of overexpressed HMGR on MCL1 and COX-II after 48 h in SW480 cells. (F) Structure of the statin hydroxamates was shown. (G) Effect of three statin hydroxamates and the corresponding statins on the cell viability of various human cancer cell lines. The half maximal inhibitory concentration (IC_{50}) values for individual cell lines are presented. Cells were treated with various concentrations of test compounds for 72 h, and cell viability was measured by the MTT assay. (H) HCT116 cells were treated with the indicated doses of test compounds for 72 h, and cell viability was measured by the MTT assay. $^{**}P < 0.01$ versus control; $^{\#}P < 0.05$ and $^{\#\#}P < 0.01$. (I) Effect of JMF3086 on the cell cycle distribution of HCT116 cells. Cells were treated with 10–50 μM JMF3086 for 24 h and analyzed by flow cytometry. (J) HCT116 cells were treated with 10 or 50 μM JMF3086 for 24 h, and terminal deoxynucleotidyl transferase dUTP nick end labeling (TUNEL) staining was performed to detect apoptotic cells. Original magnification: 400×. (K) Dose- and time-dependent effects of JMF3086 on the expression of apoptosis-related proteins in HCT116 cells. Cells were treated with 10–50 μM JMF3086 for 24 h, or treated with 10 μM JMF3086 for 24–72 h. Total cell lysates were prepared, and Western blotting was performed.

Metastatic CRC (mCRC) is an incurable disease requiring systemic drug therapy to prolong the survival of patients. Although stepwise discovery of chemotherapeutic and molecular targeted agents has improved the survival of patients with mCRC from 12 to 24 months in the past two decades (Meyerhardt and Mayer, 2005), inevitably, emerged acquired resistance ultimately leads to mortality. This introduces an unmet medical need for the discovery of new drugs. Therefore, the development of drugs with different mechanisms to avoid cross-resistance is crucial to further prolong the survival of patients with mCRC.

In this study, we demonstrated that HMGR activity was increased in CRC patients and verified as an oncotarget through knockout by CRISPR and knockdown by shRNA in HMGR-high-expressing HCT116 cells, and overexpression in HMGR-low-expressing SW480 cells. Furthermore, HMGR enhanced the stemness of CRC. JMF3086 most regulated the genes in CRC cells related to apoptosis and inflammation through a genome-wide ChIP-on-chip analysis categorized by Gene Ontology (GO). Ingenuity Pathways Analysis (IPA) analysis further predicted their respective regulation by NR3C1 and NF-κB. JMF3086 down-regulated

Fig. 2. Genome-wide analysis of target genes in JMF3086-treated HCT116 colorectal cancer cells. The cell lysates from HCT116 cells treated with 30 μM JMF3086 for 24 h were immunoprecipitated with control rabbit IgG or anti-H3K27-Ac antibody. ChIP-on-chip assays were performed, and genes with more than two-fold decrease or increase in H3K27-Ac in log-ratios were analyzed by Gene Ontology (GO). The most significant biological functions regulated by JMF3086 were apoptosis and inflammation (A–C). (A) Schematic overview of working model (upper left panel). Ingenuity Pathways Analysis (IPA) predicted that the genes associated with apoptosis were regulated by NR3C1. $P = 4.30E\text{-}37$. (B) IPA analysis predicted inflammatory genes were regulated by NF-κB. The molecular network has a P-score ($-\log_{10}$ (*P*-value)) of 48. (C) Genes with two-fold downregulation of H3K27-Ac in log-ratio are shown in green, while those with two-fold upregulation are shown in red. (D) ChIP-qPCR was performed by immunoprecipitation with control rabbit IgG or anti-H3K27-Ac, anti-CBP, anti-HDAC1, or anti-HDAC3 antibodies to detect their differential binding to the promoters of TNF-α, CD166, COX-II, BCL-2, TIMP3, and BMP2. Data were analyzed by the Q-PCR and plotted as percent (%) of input DNA. $^{*}P < 0.05$, $^{**}P < 0.01$ versus basal, two-sided Student *t*-test.

A

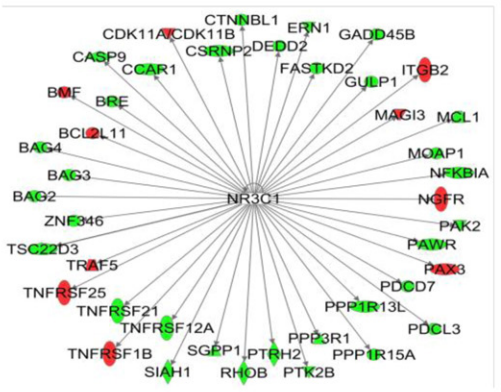

B

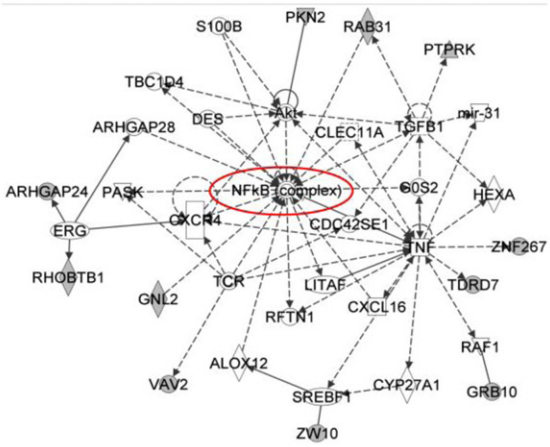

C

	Symbol	Location (Chr.)	Accession No.	H3K27 -Ac
Inflammation and proliferation				
TNF-α	TNFA	6	NM_000594.2	
CXCL1	CXCL1	4	NM_001511.3	
CXCL2	CXCL2	4	NM_002089	
COX-II	PTGS2	1	NM_000963.2	
Cyclin D1	CCND1	11	NM_053056	
Cancer stem cell				
CD166	ALCAM	3	NM_001243280.1	
EpCAM	EPCAM	2	NM_002354.2	
CD44	CD44	11	NM_000610.3	
Anti-apoptosis				
BCL2	BCL2	18	NM_000633.2	
MCL1	MCL1	1	NM_001197320.1	
Tumor suppressor				
TIMP3	TIMP3	22	NM_000362.4	
BMP2	BMP2	20	NM_001200.2	
P53	TP53	17	NM_000546.5	

D

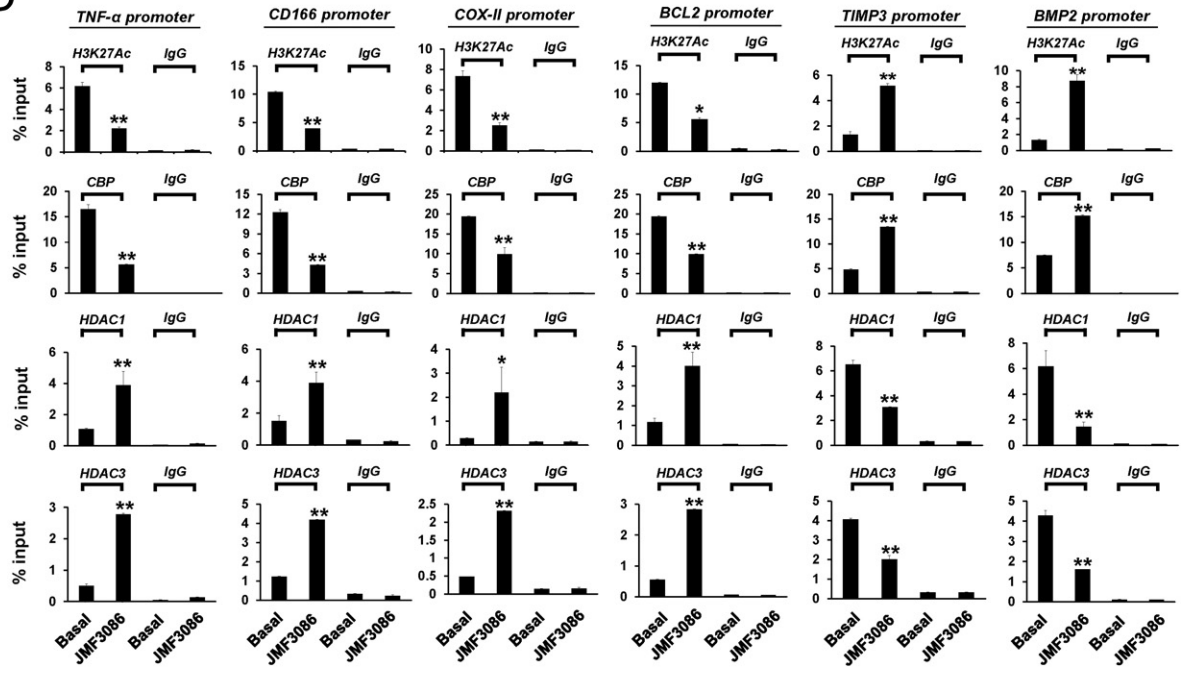

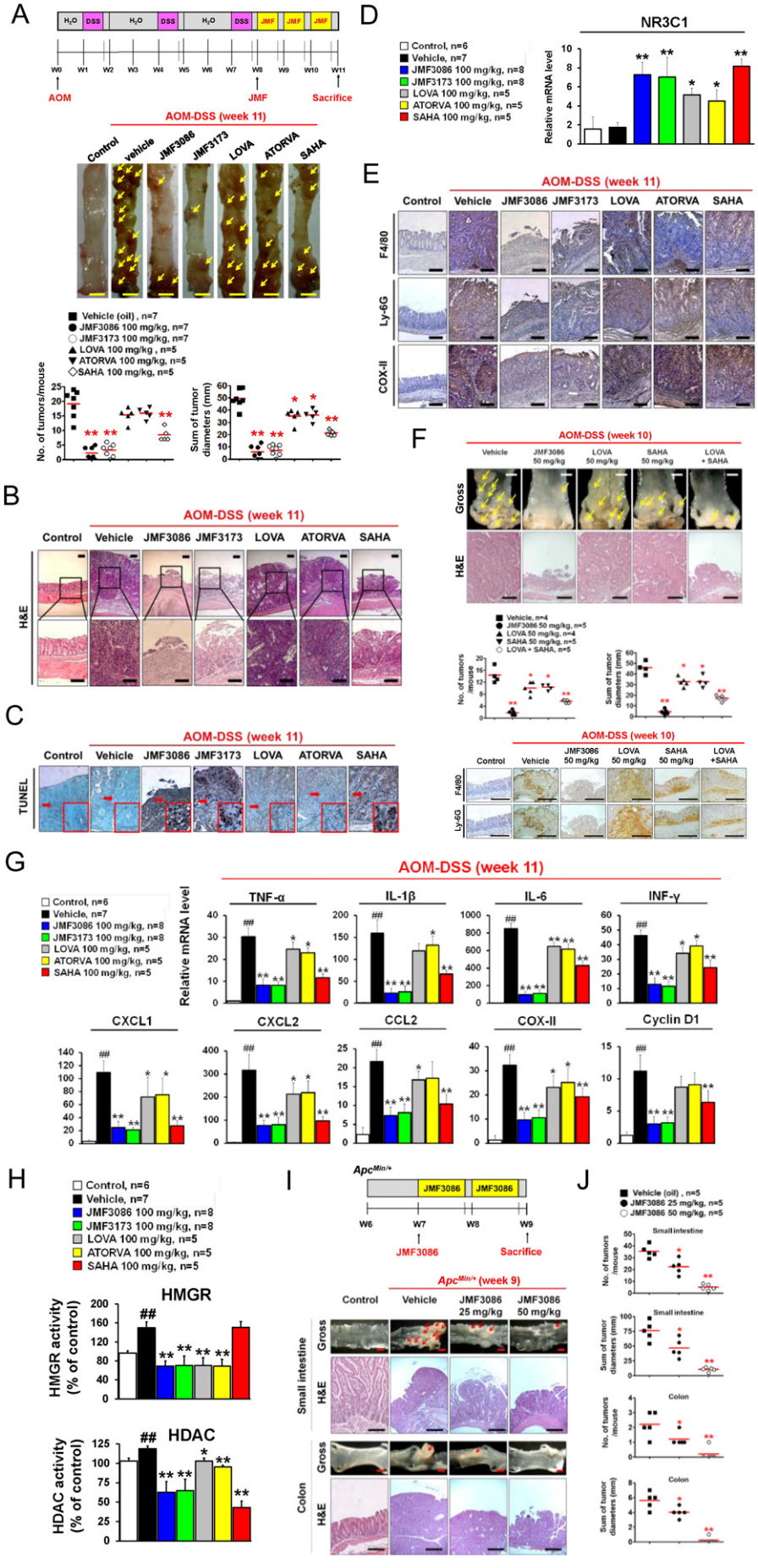
A
AOM
JMF
Sacrifice
AOM-DSS (week 11)
Control
Vehicle
JMF3086
JMF3173
LOVA
ATORVA
SAHA
Vehicle (oil) , n=7
JMF3086 100 mg/kg, n=7
JMF3173 100 mg/kg, n=7
LOVA 100 mg/kg , n=5
ATORVA 100 mg/kg, n=5
SAHA 100 mg/kg, n=5
No. of tumors/mouse
Sum of tumor diameters (mm)
B
AOM-DSS (week 11)
H&E
C
AOM-DSS (week 11)
TUNEL
D
NR3C1
Control, n=6
Vehicle, n=7
JMF3086 100 mg/kg, n=8
JMF3173 100 mg/kg, n=8
LOVA 100 mg/kg, n=5
ATORVA 100 mg/kg, n=5
SAHA 100 mg/kg, n=5
Relative mRNA level
E
AOM-DSS (week 11)
F4/80
Ly-6G
COX-II
F
AOM-DSS (week 10)
Vehicle
JMF3086 50 mg/kg
LOVA 50 mg/kg
SAHA 50 mg/kg
LOVA + SAHA
Gross
H&E
Vehicle, n=4
JMF3086 50 mg/kg, n=5
LOVA 50 mg/kg, n=4
SAHA 50 mg/kg, n=5
LOVA + SAHA, n=5
No. of tumors /mouse
Sum of tumor diameters (mm)
AOM-DSS (week 10)
Control
Vehicle
JMF3086 50 mg/kg
LOVA 50 mg/kg
SAHA 50 mg/kg
LOVA +SAHA
F4/80
Ly-6G
G
AOM-DSS (week 11)
Control, n=6
Vehicle, n=7
JMF3086 100 mg/kg, n=8
JMF3173 100 mg/kg, n=8
LOVA 100 mg/kg, n=5
ATORVA 100 mg/kg, n=5
SAHA 100 mg/kg, n=5
Relative mRNA level
TNF-α
IL-1β
IL-6
INF-γ
CXCL1
CXCL2
CCL2
COX-II
Cyclin D1
H
Control, n=6
Vehicle, n=7
JMF3086 100 mg/kg, n=8
JMF3173 100 mg/kg, n=8
LOVA 100 mg/kg, n=5
ATORVA 100 mg/kg, n=5
SAHA 100 mg/kg, n=5
HMGR
HMGR activity (% of control)
HDAC
HDAC activity (% of control)
I
ApcMin/+
JMF3086
JMF3086
W6
W7
W8
W9
JMF3086
Sacrifice
ApcMin/+ (week 9)
Control
Vehicle
JMF3086 25 mg/kg
JMF3086 50 mg/kg
Small intestine
Gross
H&E
Colon
Gross
H&E
J
Vehicle (oil) , n=5
JMF3086 25 mg/kg, n=5
JMF3086 50 mg/kg, n=5
Small intestine
No. of tumors /mouse
Small intestine
Sum of tumor diameters (mm)
Colon
No. of tumors /mouse
Colon
Sum of tumor diameters (mm)

inflammatory and stemness genes and up-regulated tumor suppressor genes. JMF3086 exhibited therapeutic benefits against azoxymethane-dextran sulfate sodium (AOM-DSS) CRC and infiltrations of macrophages and neutrophils in mice, and inhibited tumor progression in $Apc^{Min/+}$ mice as well as inhibiting the metastatic ability of CRC and angiogenesis. Furthermore, JMF3086 inhibited the stemness of CRC and potentiated the anti-cancer effect of oxaliplatin in vitro and in vivo. Our data provides compelling evidence that HMGR is an oncotarget of CRC and the polypharmacological HDAC inhibitors-statin hydroxamates we have developed exert significant therapeutic benefits in preclinical models and are promising drugs for CRC treatment.

2. Methods

2.1. Patients and Tumor Specimens

Paired tumor and control tissue samples were collected from 13 CRC patients who underwent surgical resection at National Taiwan University Hospital between 2010 and 2011. The control samples were from the normal mucosa adjacent to tumors. All samples were stored at −80 °C. The Institutional Review Board of the National Taiwan University Hospital approved the procedures for tissue collection and analysis, and written informed consent was obtained from each patient.

2.2. Mice

C57BL/6, BALB/c and NOD/SCID mice were obtained from the National Laboratory Animal Center (Taiwan). Experiments on mice were performed in accordance with protocols approved by the Institutional Animal Care and Use Committee (IACUC) of the College of Medicine, National Taiwan University.

The B6.Rcc.B6J-Apc^{Min}/Cnrm males were purchased from The European Mouse Mutant Archive (EMMAID: 02000; München, Germany). $Apc^{Min/+}$ mice were produced and maintained by breeding $Apc^{Min/+}$ males with C57BL/6 female mice.

2.3. Chromatin Immunoprecipitation (ChIP) and ChIP-on-chip Assays

HCT116 cells were treated with 30 μM JMF3086 for 24 h, and ChIP assays using control Rabbit IgG (sc-2027; Santa Cruz) or anti-H3K27-ac antibodies (#4353; Cell Signaling) were performed as previously described (Chou et al., 2011). ChIP-on-chip assays were performed in the Microarray and Gene Expression Analysis Core Facility of the National Yang-Ming University VGH Genome Research Center in Taiwan using the SurePrint G3 Human Promoter 1 × 1 M Kit (Agilent Technologies) after DNA was further purified through phenol-chloroform-isoamyl alcohol extraction and ethanol precipitation. Genes with two-fold down-regulation or upregulation of H3K27-Ac in log-ratio after JMF3086 treatment were regarded significant.

2.4. Animal Models for AOM-DSS-induced CRC

CRC was induced by intraperitoneal injection of AOM (12.5 mg/kg) in conjunction with the DSS stimulus, resulting in tumor development restricted to the colon in mice as previously described (Yang et al., 2013). Mice were maintained with a regular diet and drinking water for 7 days and then subjecting to 3 cycles of DSS treatment, with each cycle consisting of the administration of 3.5% DSS for 5 days followed by a 14-day recovery period with regular water (Fig. 3A). Body weight, the presence of occult or gross blood in the rectum, and stool consistency were determined daily in the mice. Weight change during the experiment was calculated as the percent change in weight compared with the baseline measurement. Bleeding was scored as 0 when there was no blood in the Hemoccult test, 1 for a positive Hemoccult result, 2 for slight bleeding, or 3 for gross bleeding. Regarding stool consistency, 0 points were given for well-formed pellets, 1 point for semi-formed stools that did not adhere to the anus, 2 points for pasty stools, and 3 points for liquid stools that adhered to the anus. This model is widely utilized to recapitulate human CRC because it results in inflammation and ulceration of the entire colon, similar to what is observed in patients (Ullman and Itzkowitz, 2011). Test compounds were orally administered 5 days a week for 3 weeks following the AOM-DSS treatment.

2.5. Animal Model for Experimental Colorectal Cancer Lung Metastasis

HCT116 cells (2×10^6) were injected intravenously into the tail vein of five-week-old female nude BALB/c mice. After two weeks, the mice were treated orally with JMF3086 (100 mg/kg) or vehicle (corn oil) five days a week for two weeks.

2.6. Animal Model for Experimental Colorectal Cancer Liver Metastasis

Seven-week-old female NOD/SCID mice were anesthetized by a continuous flow of 2%–3% isoflurane. To generate the mouse models with liver metastases derived from human colorectal cancer cells, HT29-Luciferase-expressing cells (1×10^6) were suspended in 100 μL PBS and injected into the spleen of mice. After a one-week recovery, the mice were randomized into vehicle or treatment groups. JMF3086 was dissolved in corn oil and administered orally five days a week for two weeks. Mice were then given endotoxin-free luciferase substrate and photographed by IVIS imaging system (Xenogen) once a week. Mice were sacrificed, and tumors from their spleens and livers were collected, weighed, and fixed by formalin.

2.7. Animal Model for Colorectal Cancer Xenograft

Female BALB/c nude mice (6–7-week-old) were injected with 10^7 HCT116 cells (suspended in 0.1 mL PBS) in the rear left flank. One week after administration, mice carried 100 to 200 mm^3 tumors were treated with vehicle, oxaliplatin (2.5 mg/kg intraperitoneally once a week), JMF3086 (10 mg/kg per oral once daily, five days per week), or

Fig. 3. Therapeutic effect of JMF compounds on colitis-induced colorectal cancer and $Apc^{Min/+}$ mouse models. (A–G) Test compounds were dissolved in corn oil and administered orally five days a week for three weeks following the AOM-DSS treatment. (A) Schematic overview of the experimental design (upper panel). Representative whole colons were depicted, and the arrowhead indicates macroscopic polyps (middle panel). Scale bars: 5 mm. The number of tumors and tumor sizes are graphed (lower panel). $^{*}P < 0.05$ and $^{**}P < 0.01$ versus vehicle. (B) Colon sections were counterstained with H&E, and high-magnification images of the black-boxed areas are shown in the lower row. Scale bar: 250 μm. (C) Colon sections from CRC mice were stained by TUNEL assay to detect apoptotic cells. The insets indicated by arrows show higher magnification images of the cells (original magnification: 400×; higher magnification: 1000×). (D) Q-PCR analysis of NR3C1 mRNA expression normalized to GAPDH in colon tissues from CRC mice is shown (lower panel). $^{*}P < 0.05$ and $^{**}P < 0.01$ versus vehicle. (E) Colon sections were immunostained with anti-F4/80, anti-Ly-6G, or anti-COX-II antibodies. Scale bar: 250 μm. (F) Gross pictures of terminal colons are shown, and arrowheads indicate macroscopic lesions. Scale bars: 5 mm. Colon sections were counterstained with H&E. Scale bars: 250 μm. The number of tumors and tumor sizes are graphed (middle panel). $^{*}P < 0.05$ and $^{**}P < 0.01$ versus vehicle. Colon sections were immunostained with anti-F4/80, or anti-Ly-6G antibodies (lower panel). Scale bar: 250 μm. (G) Colonic cytokines, chemokines, COX-II, and cyclin D1 mRNA levels were quantified by Q-PCR, and the levels of mRNA were normalized to GAPDH. Error bars represent SD. $^{\#\#}P < 0.01$ versus control; $^{*}P < 0.05$ and $^{**}P < 0.01$ versus vehicle; two-sided Student *t*-test. (H) HMGR and HDAC activities in cell lysates from colon tissues are shown. $^{\#\#}P < 0.01$ versus control; $^{*}P < 0.05$ and $^{**}P < 0.01$ versus vehicle. (I) Therapeutic effect of JMF3086 on $Apc^{Min/+}$ mice. Schematic overview of the experimental design (upper panel). Gross pictures of small intestine (middle panel) and colon (lower panel) are shown. Scale bars: 5 mm. The sections were counterstained with H&E (lower row of scale bars: 50 μm). (J) The number of tumors and tumor sizes of small intestine and colon in $Apc^{Min/+}$ mice are graphed. $^{*}P < 0.05$ and $^{**}P < 0.01$ versus vehicle.

a combination for two weeks, then sacrificed. Tumors were collected, weighed, and fixed by formalin.

2.8. Additional Methods

Detailed methodology is described in the Supplementary material.

3. Results

3.1. HMGR Is an Oncotarget of Colorectal Cancer

We examined HMGR activity in CRC patients and found an increase in CRC tissues compared to the adjacent normal epithelium (Fig. 1A and Table S1). The expression of HMGR protein in HCT116, RKO and SW480 CRC cells was examined, and high expression in HCT116 while low expression in SW480 cells was seen (Fig. 1B). To clarify the role of HMGR in CRC, CRISPR technology was utilized to establish HMGR-knockout stable clones in HCT116 cells. The apoptotic cells (suspension) were removed during maintenance, and the anti-apoptotic protein, MCL1 was found a significant reduction (Fig. 1C, left). To verify the anti-apoptotic role of HMGR, transient knockdown of HMGR by shRNA was performed. Similar to CRISPR knockout cells, MCL1 was reduced while the apoptotic proteins, BAX and cleavage of pro-caspase-3 were induced (Fig. 1C, right). To determine whether the cytotoxic effect observed in HMGR-depleted cells was due to the disruption of mevalonate pathway, HMGR-knockout stable clones were treated with mevalonate and subjected to MTT assay. Cell viability was reduced in HMGR-knockout stable clones, E6 and H5, whereas this effect was reversed by the addition of mevalonate (Fig. 1D). This data indicated that HMGR plays a pivotal role in the cell survival of CRC. On the other hand, overexpression of HMGR in SW480 cells induced MCL1 and COX-II expression (Fig. 1E). These results demonstrate the oncogenic role of HMGR in CRC cells.

The three statin hydroxamates, JMF3086, JMF3171, and JMF3173 were cytotoxic to CRC and various cancer cell lines (Fig. 1F–1G and Table S2). Addition of mevalonate partially reversed JMF3086-induced growth inhibition, but completely reversed that of lovastatin in HCT116 cells (Fig. 1H), indicating that both HMGR and HDAC inhibitions contributed to the cytotoxic effect of JMF3086. JMF3086 induced apoptosis by sub-G1 increase and cleavages of PARP and pro-caspase 3 in HCT116 cells, in which increased pro-apoptotic BAX and decreased anti-apoptotic BCL-2 were also seen (Fig. 1I–1K).

3.2. Genome-wide Analysis of JMF3086-targeted Genes in Colorectal Cancer Cells

Chromatin immunoprecipitation (ChIP)-on-chip analysis revealed the binding of H3K27-acetylation to >10,000 genes altered by JMF3086. Those with two-fold downregulation or upregulation in log-ratio were selected and analyzed by Gene Ontology (GO), which categorized them into different biological functions; the most significant ones were apoptosis and inflammation. Ingenuity Pathways Analysis (IPA) predicted their regulation by NR3C1 and NF-κB, respectively (Fig. 2A and B). JMF3086 inhibited the binding of H3K27-Ac to the promoters of genes controlling inflammation and proliferation, stemness of cancer, and anti-apoptosis, and also reduced their mRNA expression. Conversely, JM3086 increased the binding of H3K27-Ac to the gene promoters of tumor suppressors and also increased their mRNA expression (Fig. 2C and S1A–S1C). To further investigate these differential effects, the binding of acetyl-H3K27, CBP, HDAC1, and HDAC3 to promoters was examined by quantitative ChIP (qChIP) assays. JMF3086 reduced the binding of acetyl-H3K27 and CBP to the promoters of TNF-α, CD166, COX-2, BCL2, CXCL1, CXCL2, EpCAM, CD44, CyclinD1, and MCL1, but increased the binding of HDAC1 and HDAC3 to the same promoters (Fig. 2D and S1D). In contrast, JMF3086 increased the binding of acetyl-H3K27 and CBP to the promoters of TIMP3, BMP2, and p53, but decreased the binding of HDAC1 and HDAC3 to the same promoters (Fig. 2D and S1D).

3.3. JMF3086 and JMF3173 Are Effective Against Colorectal Cancer in the AOM-DSS and $Apc^{Min/+}$ Mouse Models

To investigate the in vivo anti-CRC effect of statin hydroxamates, JMF3086 (100 mg/kg) or JMF3173 (100 mg/kg, 5 days per week for 3 weeks) was orally administered after CRC tumors were induced by AOM and DSS (8th week) in mice (Fig. 3A). JMF compounds inhibited the number and size of colon tumors, as well as symptoms (i.e. body weight loss, diarrhea, and rectal bleeding), but not the shortening of colon length (Fig. 3A and S2A–S2C). Microscopically, JMF compounds inhibited AOM-DSS-induced colon adenocarcinoma with dysplasia, exhibited surface tumor necrosis by H&E staining, and induced apoptosis of CRC tumors, and also induced NR3C1 mRNA expression in the tumors (Fig. 3B–3D and S2D).

The tumor microenvironment plays an important role in cancer progression and metastasis (Popivanova et al., 2009; Hanahan and Weinberg, 2011). Tumor-associated macrophages (TAMs) and tumor-associated neutrophils (TANs) are key components of tumor microenvironment (Noy and Pollard, 2014; Mantovani, 2009). Therefore, IHC was performed in tumor section stained with the macrophage marker F4/80, neutrophil marker Ly-6G or anti-COX-II antibody (Erreni et al., 2011; Jamieson et al., 2012) (Fig. 3E and S2E). The infiltrations of macrophages and neutrophils as well as COX-II were abundant in AOM-DSS CRC and were blocked by JMF compounds but not by statins or SAHA (Fig. 3E). The anti-tumor effect of JMF3086 was superior to lovastatin plus SAHA which was ineffective to block the infiltrations of macrophages and neutrophils (Fig. 3F, bottom).

JMF compounds also reduced the mRNA expression of pro-inflammatory cytokines, chemokines, COX-II, and cyclin D1 in the colon (Fig. 3G). Both HMGR and HDAC activities elevated after AOM-DSS-induced tumors were inhibited by JMF compounds, and the extent of inhibition correlated with reductions in tumor number and size (Fig. 3H, S3A, and S3B). In addition, the anti-cancer and anti-inflammatory effects of JMF compounds were better than those of SAHA or statins (Fig. 3A–3F). These indicated that both HDAC and HMGR contributed to the effects of JMF compounds.

In addition to the AOM-DSS model, which is a representative of inflammation-induced CRC, the effect of JMF3086 was examined in the *Min* (multiple intestinal neoplasia) mouse model. The *Min* model is the most commonly used transgenic CRC model, carrying a point

Fig. 4. Therapeutic effect of JMF3086 on colorectal cancer metastasis to the lung and liver in vivo. (A) Schematic overview of the experimental design (upper left panel). Gross pictures of lungs (scale bars: 5 mm) and their sections counterstained with H&E (scale bars: 250 μm) are shown (middle panel). Quantitation of metastatic tumor nodules in mice are presented (upper right panel). $^{**}P < 0.01$ versus vehicle. (B) HMGR and HDAC activities in cell lung lysates are shown. $^{\#\#}P < 0.01$ versus control; $^{**}P < 0.01$ versus vehicle. (C) Schematic overview of the experimental design (upper left panel). The luciferase activity was detected by the IVIS imaging system three weeks after JMF3086 treatment (lower panel) and quantitative data are shown (upper right panel). (D) Bioluminescence images of dissected spleens and livers from each mouse are shown (left panel). Synchronized images were quantified (right panel). $^{**}P < 0.01$ versus vehicle. (E) Gross pictures of spleen (upper panel) and liver (lower panel) are shown. The arrowheads indicate macroscopic tumor nodules (scale bar: 5 mm). Spleen and liver sections were counterstained with H&E in the lower row (scale bars: 50 μm). (F) The number of liver nodules was graphed three weeks after JMF3086 treatment. $^{**}P < 0.01$ versus vehicle. (G) HCT116 cells treated with 30 μM JMF3086 for 20 h were exposed to hypoxia for 4 h, then conditioned media was collected and the matrigel plug assay was performed. We mixed 75 μL of conditioned media with 425 μL matrigel and 50 U heparin/mL was subcutaneously injected into nude mice, which were sacrificed and dissected after 14 days. Quantification of neovessel formation in matrigel plugs was estimated using Drabkin reagent kit 525. Matrigel plugs retrieved from mice were photographed. RPMI medium served as a negative control. $^{\#\#}P < 0.01$ versus normoxia; $^{**}P < 0.01$ versus hypoxia.

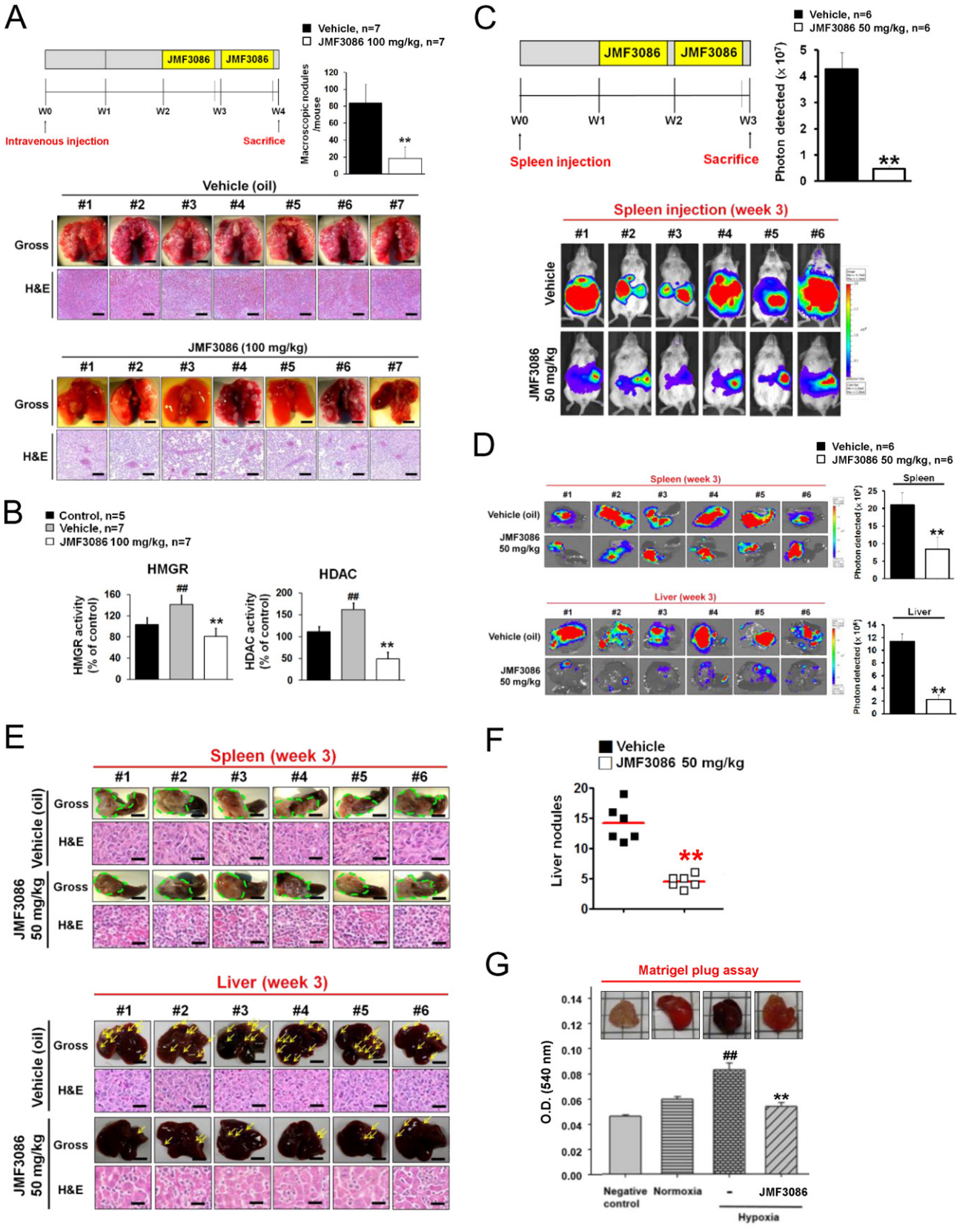

mutation in the *Apc* gene and developing small intestinal and colon tumors between five and eight weeks. Germline mutations of *Apc* in humans will lead to colon polyposis and a cancer termed familial adenomatous polyposis (FAP) (Moser et al., 1990; Kettunen et al., 2003; Shibata et al., 1997). JMF3086 (25 mg/kg or 50 mg/kg) inhibited tumor formation in the small intestine and colon of $Apc^{Min/+}$ mice (Fig. 3I–3J).

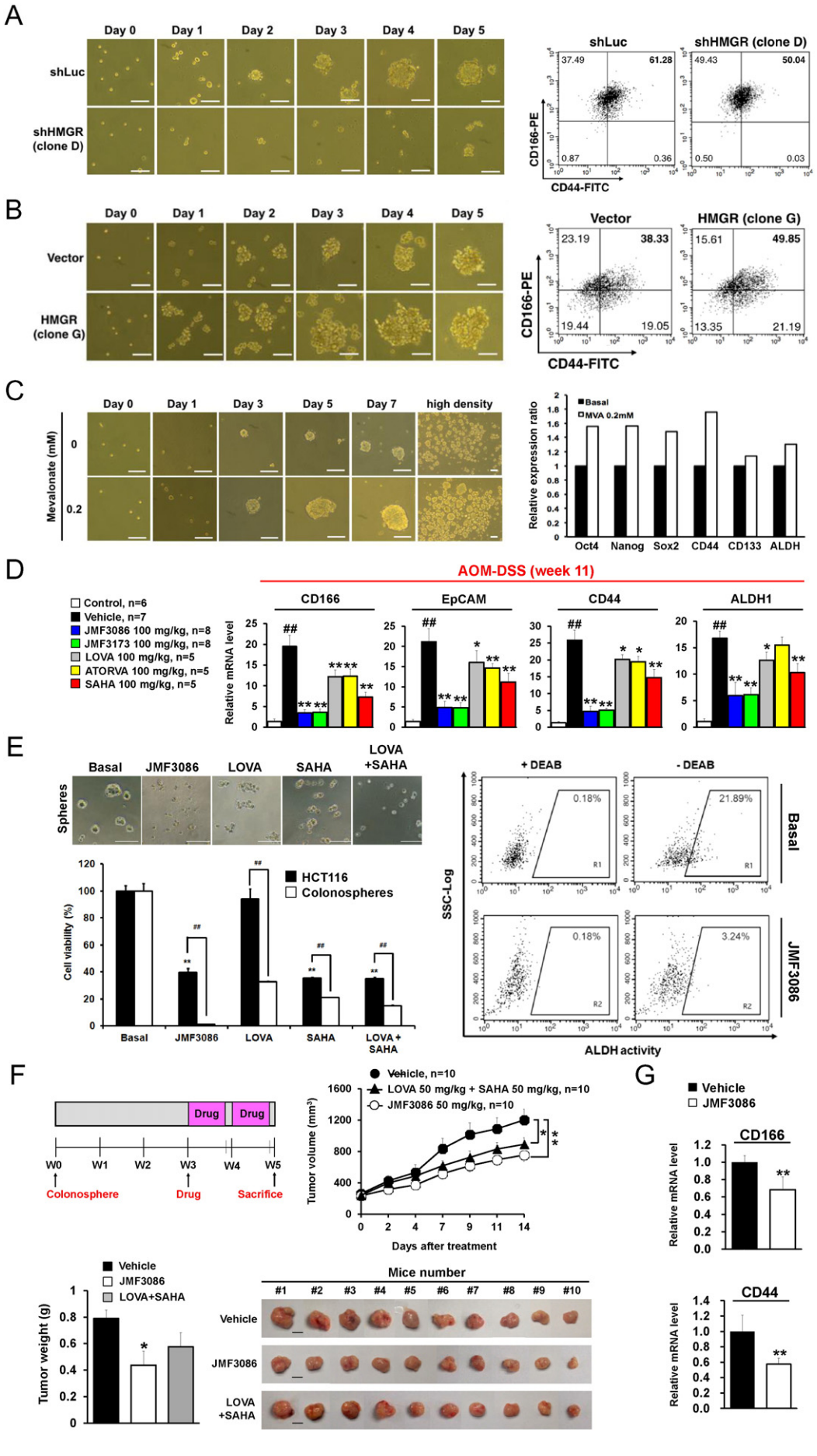
A
Day 0
Day 1
Day 2
Day 3
Day 4
Day 5
shLuc
shHMGR (clone D)
shLuc
shHMGR (clone D)
37.49
61.28
0.87
0.36
49.43
50.04
0.50
0.03
CD166-PE
CD44-FITC
B
Vector
HMGR (clone G)
Vector
HMGR (clone G)
23.19
38.33
19.44
19.05
15.61
49.85
13.35
21.19
C
Day 0
Day 1
Day 3
Day 5
Day 7
high density
Mevalonate (mM)
0
0.2
Basal
MVA 0.2mM
Relative expression ratio
Oct4
Nanog
Sox2
CD44
CD133
ALDH
D
AOM-DSS (week 11)
Control, n=6
Vehicle, n=7
JMF3086 100 mg/kg, n=8
JMF3173 100 mg/kg, n=8
LOVA 100 mg/kg, n=5
ATORVA 100 mg/kg, n=5
SAHA 100 mg/kg, n=5
CD166
EpCAM
CD44
ALDH1
Relative mRNA level
E
Basal
JMF3086
LOVA
SAHA
LOVA +SAHA
Spheres
HCT116
Colonospheres
Cell viability (%)
+ DEAB
- DEAB
0.18%
21.89%
0.18%
3.24%
Basal
JMF3086
SSC-Log
ALDH activity
F
Drug
Drug
W0
W1
W2
W3
W4
W5
Colonosphere
Drug
Sacrifice
Vehicle, n=10
LOVA 50 mg/kg + SAHA 50 mg/kg, n=10
JMF3086 50 mg/kg, n=10
Tumor volume (mm³)
Days after treatment
Vehicle
JMF3086
LOVA+SAHA
Tumor weight (g)
Mice number
#1
#2
#3
#4
#5
#6
#7
#8
#9
#10
Vehicle
JMF3086
LOVA +SAHA
G
Vehicle
JMF3086
CD166
CD44
Relative mRNA level

3.4. JMF3086 Inhibits the In Vivo Lung and Liver Metastases of Colorectal Cancer

Metastasis is a major cause of death from CRC, in which livers or lungs are the most frequent sites (Villeneuve and Sundaresan, 2009; Edwards et al., 2012). To examine the anti-metastatic activity of JMF3086, HCT116 cells were intravenously injected into nude mice via the tail vein. JMF3086 (100 mg/kg) reduced lung tumor nodules by macroscopic observation (Fig. 4A), indicating an inhibition on lung metastasis. Increased HMGR and HDAC activities in metastatic lung tumors were inhibited by JMF3086 (Fig. 4B), and the extent of inhibitions was correlated with the effect of anti-lung metastasis (Fig. S4A and S4B). The accumulation of JMF3086 in metastatic tumor cells in lungs was also seen (Fig. S4C–S4E).

A liver metastasis model was established using HT29-Luciferase-expressing cells injected into the spleen of NOD/SCID mice, which were photographed by the IVIS imaging system (Fig. 4C). Ex vivo bioluminescence in excised spleens and livers detected by IVIS showed that JMF3086 inhibited liver metastasis and primary tumor growth in spleens (Fig. 4C–4F and S4F). H&E staining further confirmed these findings (Fig. 4E). JMF3086 did not influence body weight (Fig. S4G).

Angiogenesis is an essential step in tumor growth and metastasis (Ellis and Hicklin, 2008). Conditioned medium from HCT116 cells under hypoxia induced angiogenesis by matrigel plug assay in mice, the effect of which was inhibited by JMF3086 (Fig. 4G), indicating its anti-angiogenic effect.

3.5. HMGR Enhances Colorectal Cancer Stemness and JMF3086 Inhibits Stemness In Vitro and In Vivo

Stem cell expansion derived from the chronic inflammation of colon which causes crypt injury and regeneration contributes to the genesis, maintenance, recurrence, metastasis, and drug resistance of CRC (Eyler and Rich, 2008; Pignalosa and Durante, 2012), and CD166, EpCAM, CD44, and ALDH1 are putative surface markers (Huang and Wicha, 2008). CRC stem cells were generated by spheroid formation in suspension cultured from HCT116 cells (Mani et al., 2008) (Fig. S5A–S5F). Knockdown of HMGR in HCT116 cells reduced the generation of spheroid formation and the proportion of CD44/CD166 positive cells (Fig. 5A). In contrast, overexpression of HMGR in SW480 cells enhanced the spheroid formation and the proportion of CD44/CD166 positive cells (Fig. 5B). Addition of mevalonate to HMGR-low-expressing LS-174 T cells showed a similar result (Fig. 5C). These results indicate a role of HMGR in CRC stemness.

The mRNA expression of CRC stemness markers was increased in AOM-DSS-CRC mice and inhibited by JMF compounds (Fig. 5D). The formation of colonospheres as well as $ALDH^+$ population was inhibited by JMF3086 (Fig. 5E). JMF3086 also suppressed the tumor growth and tumor mass arising from colorectal CSCs in vivo, and inhibited the expression of CD166 and CD44 in the excised tumors (Fig. 5F–5G). Here, JMF3086 was superior to lovastatin plus SAHA (Fig. 5F). These data demonstrated the effectiveness of JMF3086 to inhibit the stemness of CRC in vitro and in vivo.

3.6. JMF3086 Potentiated the Anti-cancer Effect of Oxaliplatin on Colorectal Cancer In Vitro and In Vivo

Chemotherapy remains an important treatment option for metastatic CRC, and drug combination is a rational approach to further improve its efficacy (Chibaudel et al., 2012; Meyerhardt and Mayer, 2005). Therefore, we combined JMF3086 with oxaliplatin to examine their effect on CRC cells. Oxaliplatin-induced inhibition of cell viability in HCT116 cells was potentiated by JMF3086, accompanied by enhanced cleavages of PARP and pro-caspase 3, as well as an increase in sub-G1 population (Fig. 6A–6C).

We further examined the efficacy of JMF3086 combined with oxaliplatin in various mouse models. Oxaliplatin (2.5 mg/kg) plus JMF3086 (10 mg/kg) showed enhanced effect on reducing the size and weight of HCT116 xenograft tumors. Enhanced apoptosis in xenografted tumors without influencing the body weight was seen (Fig. 6D–6F, S6A, and S6B). The combination efficacy (JMF3086 25 mg/kg and oxaliplatin 5 mg/kg) was also examined in the AOM-DSS-CRC mouse model (Fig. 6G). The number and size of tumors attenuated by oxaliplatin or JMF3086 alone were further reduced by their combination (Fig. 6G, H, and S6C). Microscopically, AOM-DSS-induced colon adenocarcinoma with dysplasia was recovered to tumor necrosis in combination-treated mice (Fig. 6H). Hypoxia detected by HIF-1α and hypoxyprobe seen in colon adenocarcinomas was reduced by combination (Fig. 6I).

The combined effect of JMF3086 with oxaliplatin on CRC liver metastasis was also examined. Oxaliplatin (2.5 mg/kg) plus JMF3086 (10 mg/kg) showed better activity against tumors in spleen and liver than either drug alone (Fig. 7A–7C and S6D). H&E staining further confirmed these findings (Fig. 7D), while body weight was not affected (Fig. S6E).

4. Discussion

HMGR targeted by statins is the rate-limiting enzyme for the mevalonate pathway to synthesize cholesterol and regulate protein prenylation for cell growth (Thurnher et al., 2012). Since statins could inhibit mevalonate metabolism, they have been tested as antitumor drugs (Goldstein and Brown, 2015). Atorvastatin suppressed tumor initiation and growth in a transgenic model of MYC-induced hepatocellular carcinoma (HCC) as well as in human HCC-derived cell lines. These effects were blocked by the addition of mevalonate (Cao et al., 2011), indicating the correlation between HMGR inhibition and anti-cancer effects of statins. In this study, we further explored the role of HMGR as an oncotarget in CRC. Its knockout or knockdown in HMGR-high-expressing CRC cells reduced the anti-apoptoic but increased apoptotic proteins. However, its overexpression in HMGR-low-expressing CRC cells induced anti-apoptotic protein and COX-II expressions. Addition

Fig. 5. Role of HMG-CoA reductase in colorectal cancer stem cells and the effect of JMF3086 in vitro and in vivo. (A–C) HMGR modulated spheroids formation in colon cancer cells. (A) Effect of HMGR knockdown on spheroids formation in HCT116 cells. Sphere-formation assay following HMGR knockdown in HCT116 cells. Cell morphology was monitored by microscopy (left panel). Scale bars: 100 μm. $CD44^+/CD166^+$ population in HCT116 spheroids was quantified by flow cytometry (right panel). (B) Effect of HMGR overexpression on spheroids formation in SW480 cells. Sphere-formation assay following HMGR overexpression in SW480 cells. Cell morphology was monitored by microscopy (left panel). Scale bars: 100 μm. $CD44^+/CD166^+$ population in SW480 spheroids was quantified by flow cytometry (right panel). (C) Effect of mevalonate on spheroids formation in LS-174T cells. LS-174T cells were treated with vehicle or mevalonate 0.2 mM during in vitro sphere-formation assay. Cell morphology was monitored by microscopy (left panel). Scale bars: 100 μm. mRNA expression of stemness genes or markers were analyzed by qRT-PCR (right panel). (D) The mRNA expression of colorectal cancer stem cell markers in colon tissues from 11-week AOM-DSS-CRC mice are shown. $^{\#\#}P < 0.01$ versus control; $^{*}P < 0.05$ and $^{**}P < 0.01$ versus vehicle. (E) HCT116 colonospheres were dissociated into single cells and plated at a density of 3000 cells/well in a 96-well plate. One day after plating, cells were treated with 30 μM JMF3086, lovastatin, SAHA, or the combination of lovastatin and SAHA for 48 h. Cell morphology was monitored by microscopy (upper left panel), and cell viability was measured by WST-1 assay (lower left panel). Scale bars: 100 μm. $^{**}P < 0.01$ versus basal; $^{\#\#}P < 0.01$. HCT116 cells were incubated with 30 μM JMF3086 for 24 h, and ALDH activity was measured by flow cytometry (right panel). The trapezoid (R1, R2) indicates the $ALDH^+$ population. (F) HCT116 colonospheres (2×10^4 cells) were subcutaneously implanted into nude mice. The schematic overview of the experimental period follows (upper left panel). When the tumor volume reached 200 mm^3, vehicle (oil), JMF3086 (50 mg/kg), or the combination of lovastatin (50 mg/kg) and SAHA (50 mg/kg) were orally administered for two weeks. The tumor volume was measured every two days after JMF3086 treatment (upper right panel). $^{*}P < 0.05$ versus vehicle. A comparison of xenograft tumor weight (lower left panel) and gross picture (lower right panel) are shown. Scale bars: 5 mm. $^{*}P < 0.05$ versus vehicle. (G) Q-PCR analyzed the mRNA expressions of CD166 and CD44, which were normalized to GAPDH. $^{**}P < 0.01$ versus vehicle.

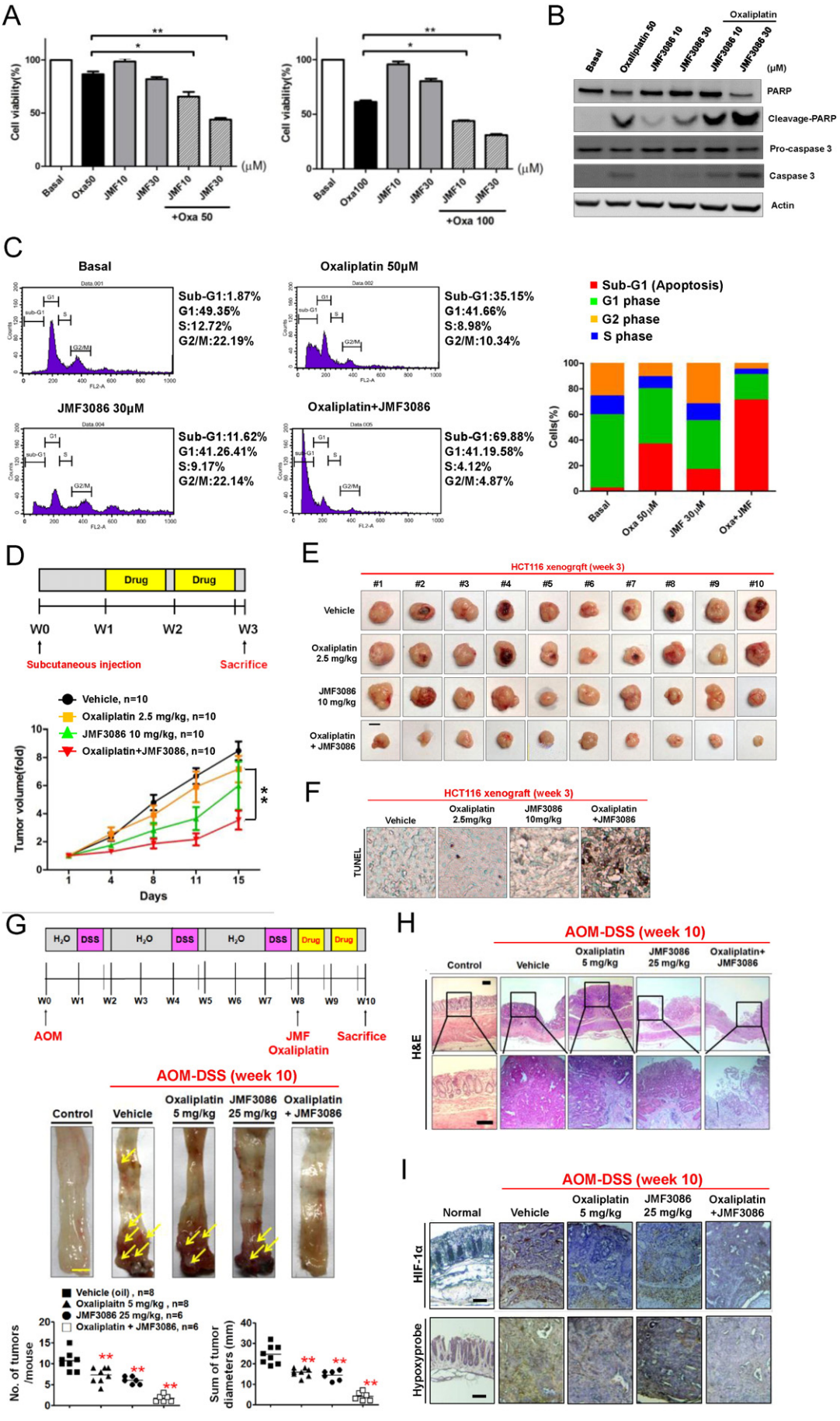
A
Cell viability(%)
Basal
Oxa50
JMF10
JMF30
JMF10
JMF30
+Oxa 50
Oxa100
+Oxa 100
(μM)
B
Oxaliplatin
Basal
Oxaliplatin 50
JMF3086 10
JMF3086 30
JMF3086 10
JMF3086 30
PARP
Cleavage-PARP
Pro-caspase 3
Caspase 3
Actin
C
Basal
Sub-G1:1.87%
G1:49.35%
S:12.72%
G2/M:22.19%
Oxaliplatin 50μM
Sub-G1:35.15%
G1:41.66%
S:8.98%
G2/M:10.34%
JMF3086 30μM
Sub-G1:11.62%
G1:41.26.41%
S:9.17%
G2/M:22.14%
Oxaliplatin+JMF3086
Sub-G1:69.88%
G1:41.19.58%
S:4.12%
G2/M:4.87%
Sub-G1 (Apoptosis)
G1 phase
G2 phase
S phase
Cells(%)
Basal
Oxa 50μM
JMF 30μM
Oxa+JMF
D
Drug
Drug
W0
W1
W2
W3
Subcutaneous injection
Sacrifice
Vehicle, n=10
Oxaliplatin 2.5 mg/kg, n=10
JMF3086 10 mg/kg, n=10
Oxaliplatin+JMF3086, n=10
Tumor volume(fold)
Days
E
HCT116 xenogrqft (week 3)
#1
#2
#3
#4
#5
#6
#7
#8
#9
#10
Vehicle
Oxaliplatin 2.5 mg/kg
JMF3086 10 mg/kg
Oxaliplatin + JMF3086
F
HCT116 xenograft (week 3)
Vehicle
Oxaliplatin 2.5mg/kg
JMF3086 10mg/kg
Oxaliplatin +JMF3086
TUNEL
G
H2O
DSS
H2O
DSS
H2O
DSS
Drug
Drug
W0
W1
W2
W3
W4
W5
W6
W7
W8
W9
W10
AOM
JMF Oxaliplatin
Sacrifice
AOM-DSS (week 10)
Control
Vehicle
Oxaliplatin 5 mg/kg
JMF3086 25 mg/kg
Oxaliplatin + JMF3086
Vehicle (oil), n=8
Oxaliplaitn 5 mg/kg, n=8
JMF3086 25 mg/kg, n=6
Oxaliplatin + JMF3086, n=6
No. of tumors /mouse
Sum of tumor diameters (mm)
H
AOM-DSS (week 10)
Control
Vehicle
Oxaliplatin 5 mg/kg
JMF3086 25 mg/kg
Oxaliplatin+ JMF3086
H&E
I
AOM-DSS (week 10)
Normal
Vehicle
Oxaliplatin 5 mg/kg
JMF3086 25 mg/kg
Oxaliplatin +JMF3086
HIF-1α
Hypoxyprobe

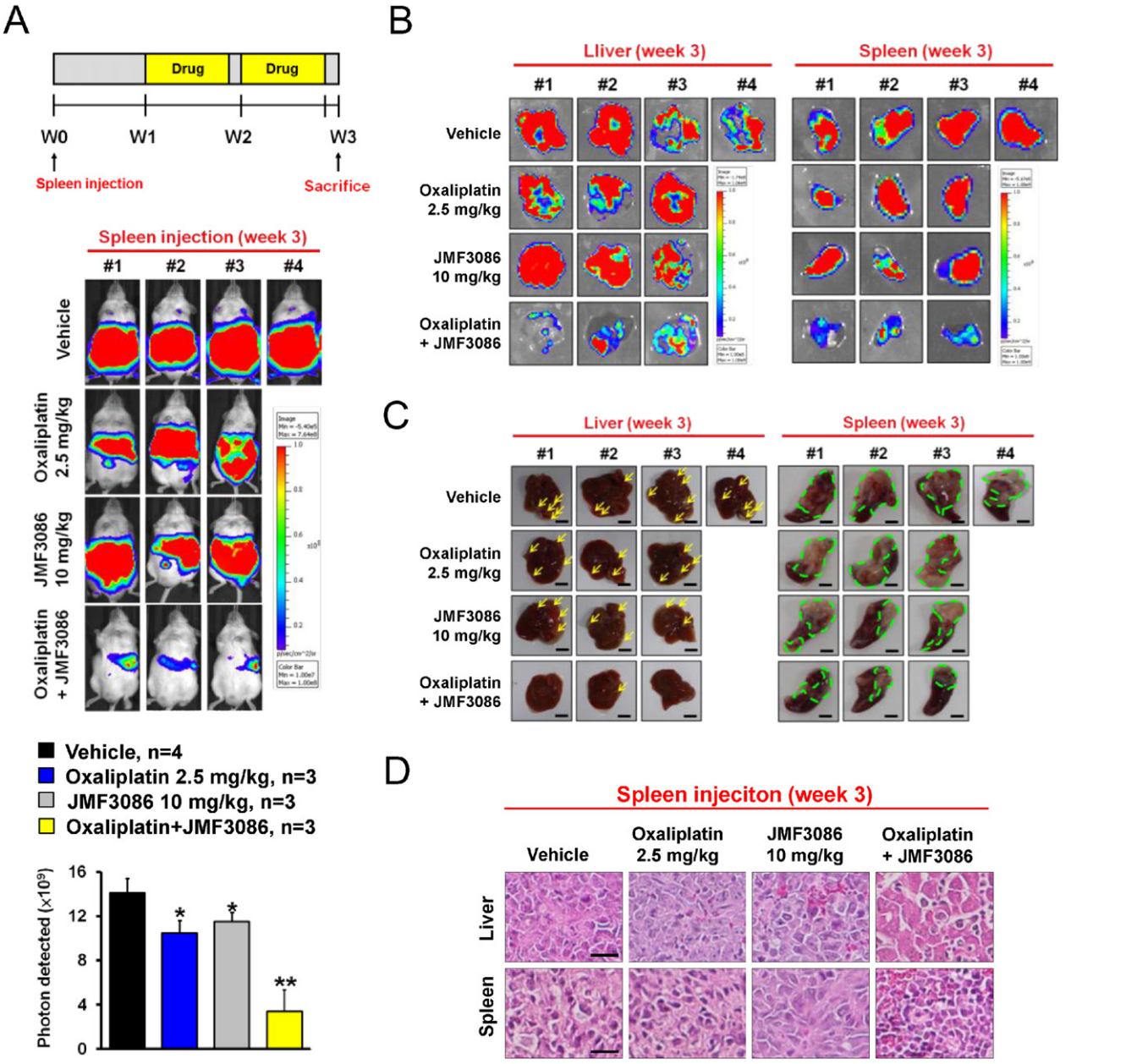

Fig. 7. Effect of JMF3086 combined with oxaliplatin on colorectal cancer metastasis to the liver in mouse models. (A) Schematic overview of the experimental design (upper panel). HT29-Luciferase-expressing cells were injected into the spleen of NOD/SCID mice. After one-week recovery, oxaliplatin (2.5 mg/kg) in combination with JMF3086 (10 mg/kg) were administered for an additional two weeks. Luciferase activity was detected three weeks after JMF3086 treatment by the IVIS imaging system (middle panel), which was then quantified (lower panel). (B) Bioluminescence images of dissected livers (left panel) and spleens (right panel) from each mouse are shown. (C) Gross pictures of liver (left panel) and spleen (right panel) are shown, with arrowheads indicating the macroscopic tumor nodules (scale bar: 5 mm). (D) Spleen and liver sections were counterstained with H&E (scale bars: 50 μm).

of mevalonate restored the cell viability of CRISPR knockout HMGR-HCT116 cells. HMGR has been reported to be a critical regulator of MYC phosphorylation, activation and tumorigenic properties in HCC cells, and MYC positively regulated the expression of HMGR in esophageal squamous carcinoma cells (Cao et al., 2011; Zhong et al., 2014).

Our previous study demonstrated that HDAC inhibition contributed to the anticancer effect of statins (Lin et al., 2008). Combining anti-cancer drugs with different mechanisms is a rational approach to improve efficacy. JMF3086, synthesized to inhibit both HDACs and HMGR, exhibits significant benefits above lovastatin plus SAHA. This advantage

Fig. 6. Potentiation of JMF3086 on the effect of oxaliplatin in vitro and in colorectal cancer mouse models in vivo. (A–C) Effect of JMF3086 combined with oxaliplatin on the cell viability, on the expression of apoptosis-related proteins, and on the cell cycle distribution are shown. (A) HCT116 cells were treated with JMF3086, oxaliplatin, or their combination for 24 h, and then cell viability was assessed by MTT assay. $^{*}P < 0.05$ and $^{**}P < 0.01$. (B) Total cell lysates were prepared, and Western blotting was performed. (C) Flow cytometry was analyzed. (D–F) Effect of JMF3086 combined with oxaliplatin on HCT116 xenograft models. (D) Schematic overview of the experimental design (upper panel). The tumor volumes were monitored for two weeks after drug treatment (lower panel). (E) Gross pictures of xenograft tumors are shown. Scale bar: 1 cm. (F) Xenograft tumors from CRC mice were stained by TUNEL assay to detect apoptotic cells (original magnification: 1000×). (G–I) Effect of JMF3086 combined with oxaliplatin on AOM-DSS-induced CRC mouse models. (G) Schematic overview of the experimental design (upper panel). Representative whole colons are depicted (middle panel), with arrowheads indicating macroscopic polyps. Scale bars: 5 mm. The number of tumors and tumor sizes are graphed. $^{**}P < 0.01$ versus vehicle (lower panel). (H) Colon sections were counterstained with H&E, and high-magnification images of the black-boxed area are shown in the lower row. Scale bar: 250 μm. (I) Colon sections were immunostained with anti-HIF-1α and anti-pimonidazole (hypoxyprobe) antibodies. Representative images from three independent experiments are presented. Scale bar: 250 μm.

is like a two-in-one antibody which is better than two monospecific antibodies (Schaefer et al., 2011). Various polypharmacological molecules dually inhibiting HDACs and other therapeutic targets have also been developed and provide an impetus to develop more anti-cancer treatments (Falkenberg and Johnstone, 2014). Evading apoptosis is a hallmark of cancer (Hanahan and Weinberg, 2011), where apoptosis induction represents one therapeutic strategy (Cotter, 2009). Anti-apoptotic genes such as BCL2 and MCL1 were down-regulated by JMF3086 from genome-wide ChIP-on-chip and Q-PCR analyses, and JMF3086 did induce apoptosis in HCT116 cells and tumors of CRC mice, indicating the contribution of apoptosis induction to the therapeutic effect of JMF3086 on CRC. NR3C1, which is a glucocorticoid receptor, was predicted to be induced by JMF3086 from GO and IPA analyses. It induced apoptotic cell death via decreasing the expression of anti-apoptotic proteins such as BCL2 and MCL1, and/or via inducing the expression of pro-apoptotic proteins such as BCL-2-like apoptosis initiator-11 (BCL2L11) (Schlossmacher et al., 2011). JMF compounds did induce NR3C1 mRNA expression in CRC mice, indicating its contribution to apoptosis.

The tumor microenvironment consisting of cancer cells, stromal tissue, blood vessels, immune cells, fibroblasts, bone marrow-derived inflammatory cells, lymphocytes and the extracellular matrix, plays a critical role in cancer development, progression and metastasis (Popivanova et al., 2009; Hanahan and Weinberg, 2011). Clinical studies have indicated its association with poor prognosis in patients with various human cancers (Erreni et al., 2011; Gregory and Houghton, 2011). Tumor-associated macrophages (TAMs) are key components of tumor microenvironment (Noy and Pollard, 2014). They can produce growth factors, cytokines, chemokines and matrix metalloproteases (MMP) to promote cancer progression, metastasis, angiogenesis and lymphangiogenesis (Qian and Pollard, 2010). Tumor-associated neutrophils (TANs) acting through the production of cytokines/chemokines and the recruitment of TAMs to the tumor sites also play a role in tumor microenvironment (Mantovani, 2009; Nathan, 2006). In this study, both infiltrations of macrophages and neutrophils occurring in AOM-DSS mouse models were blocked by JMF compounds but not by statins, SAHA or lovastatin plus SAHA (Fig. 3E and F), probably explaining the better efficacy of JMF3086 than lovastatin plus SAHA in treating AOM-DSS CRC. However, whether TAMs and TANs affected by JMF3086 are beyond its inhibitions on HMGR and HDAC remains to be investigated.

Metastasis is the major cause of CRC-related deaths, and livers or lungs are the primary organs of metastasis (Villeneuve and Sundaresan, 2009; Edwards et al., 2012). JMF3086 showed significant efficacy in inhibiting metastasis and potentiated the effect of oxaliplatin. The mechanism may involve the inhibition on angiogenesis (Fig. 4G). Furthermore, combination of JMF3086 with oxaliplatin reduced the hypoxic region and downregulated HIF-1α expression in vivo (Fig. 6I). Stemness of cancer cells may play a role in the genesis, maintenance, recurrence, metastasis, and drug resistance of CRC (Eyler and Rich, 2008; Pignalosa and Durante, 2012). Loss of CSC populations or stem-like properties could hinder the metastatic spread of the tumor (Pattabiraman and Weinberg, 2014). Stem cell expansion was derived from chronic inflammation causing damage and regeneration of crypt and release of cytokines, which maintain and regulate cancer stem-cell niche (Carpentino et al., 2009; Liu and Wicha, 2010). JMF3086 attenuated the cytokines in CRC mice and inhibited the expression of stemness-related genes. We provide direct evidences to demonstrate that HMGR enhances the stemness of CRC cells, and JMF3086 inhibited the growth of colonospheres and colonosphere-derived xenografts more than lovastatin plus SAHA. Statins was reported to lower cytokines levels to target CSCs and inhibited tumor growth as well as metastasis (Ridker et al., 2005), and HDAC inhibitor reduced the stemness of CRC cells (Kodach et al., 2011; Sikandar et al., 2010). These indicate that dual HMGR-HDAC inhibitor JMF3086-induced inhibitions on stemness and metastasis contribute to its anti-CRC effect.

In summary, our findings indicate that HMGR is an oncotarget to enhance survival and stemness of CRC. The dual HMGR-HDAC inhibitor, JMF3086, exhibits promising preclinical efficacy against CRC and its metastasis in mouse models. It also potentiates the effect of the standard chemotherapy drug oxaliplatin. Therefore, JMF3086 is a promising lead compound for CRC treatment.

Grant Support

This work was supported by a research grant from the National Science Council, Taiwan and the Institute of Biomedical Sciences, Academia Sinica (IBMS-CRC103-P02).

Conflicts of Interest

The authors disclose no conflicts of interest.

Author Contributions

Study concept and design: Chen CC
Acquisition of data: Wei TT, Lin YT, Chen WS, Luo P, Lin YH, Chen NW
Analysis and interpretation of data: Wei TT, Lin YT, Shun CT, Lin YH, Chen NW
Drafting of the manuscript: Wei TT, Chen CC
Critical revision of the manuscript for important intellectual content: Chen CC, Lin YC
Statistical analysis: Wei TT, Lin YT, Lin YH, Chen NW
Obtained funding: Chen CC
Technical or material support: Fang JM, Chen JB, Chen NW, Yang KC, Wu MS, Chang LC, Tai KY, Liang JT
Study supervision: Chen CC

Appendix A. Supplementary data

Supplementary data to this article can be found online at http://dx.doi.org/10.1016/j.ebiom.2016.07.019.

References

Cao, Z., Fan-Minogue, H., Bellovin, D.I., Yevtodiyenko, A., Arzeno, J., Yang, Q., Gambhir, S.S., Felsher, D.W., 2011. MYC phosphorylation, activation, and tumorigenic potential in hepatocellular carcinoma are regulated by HMG-CoA reductase. Cancer Res. 71, 2286–2297.
Carpentino, J.E., Hynes, M.J., Appelman, H.D., Zheng, T., Steindler, D.A., Scott, E.W., Huang, E.H., 2009. Aldehyde dehydrogenase-expressing colon stem cells contribute to tumorigenesis in the transition from colitis to cancer. Cancer Res. 69, 8208–8215.
Chen, J.B., Chern, T.R., Wei, T.T., Chen, C.C., Lin, J.H., Fang, J.M., 2013. Design and synthesis of dual-action inhibitors targeting histone deacetylases and 3-hydroxy-3-methylglutaryl coenzyme a reductase for cancer treatment. J. Med. Chem. 56, 3645–3655.
Chibaudel, B., Tournigand, C., Andre, T., de Gramont, A., 2012. Therapeutic strategy in unresectable metastatic colorectal cancer. Ther. Adv. Med. Oncol. 4, 75–89.
Chou, C.W., Wu, M.S., Huang, W.C., Chen, C.C., 2011. HDAC inhibition decreases the expression of EGFR in colorectal cancer cells. PLoS One 6, e18087.
Cotter, T.G., 2009. Apoptosis and cancer: the genesis of a research field. Nat. Rev. Cancer 9, 501–507.
Edwards, M.S., Chadda, S.D., Zhao, Z., Barber, B.L., Sykes, D.P., 2012. A systematic review of treatment guidelines for metastatic colorectal cancer. Color. Dis. 14, e31–e47.
Ellis, L.M., Hicklin, D.J., 2008. VEGF-targeted therapy: mechanisms of anti-tumour activity. Nat. Rev. Cancer 8, 579–591.
Erreni, M., Mantovani, A., Allavena, P., 2011. Tumor-associated macrophages (TAM) and inflammation in colorectal cancer. Cancer Microenviron. 4, 141–154.
Eyler, C.E., Rich, J.N., 2008. Survival of the fittest: cancer stem cells in therapeutic resistance and angiogenesis. J. Clin. Oncol. 26, 2839–2845.
Falkenberg, K.J., Johnstone, R.W., 2014. Histone deacetylases and their inhibitors in cancer, neurological diseases and immune disorders. Nat. Rev. Drug Discov. 13, 673–691.
Freed-Pastor, W.A., Mizuno, H., Zhao, X., Langerod, A., Moon, S.H., Rodriguez-Barrueco, R., Barsotti, A., Chicas, A., Li, W., Polotskaia, A., Bissell, M.J., Osborne, T.F., Tian, B., Lowe, S.W., Silva, J.M., Borresen-Dale, A.L., Levine, A.J., Bargonetti, J., Prives, C., 2012. Mutant p53 disrupts mammary tissue architecture via the mevalonate pathway. Cell 148, 244–258.
Goldstein, J.L., Brown, M.S., 2015. A century of cholesterol and coronaries: from plaques to genes to statins. Cell 161, 161–172.
Gregory, A.D., Houghton, A.M., 2011. Tumor-associated neutrophils: new targets for cancer therapy. Cancer Res. 71, 2411–2416.

Hanahan, D., Weinberg, R.A., 2011. Hallmarks of cancer: the next generation. Cell 144, 646–674.
Huang, E.H., Wicha, M.S., 2008. Colon cancer stem cells: implications for prevention and therapy. Trends Mol. Med. 14, 503–509.
Jamieson, T., Clarke, M., Steele, C.W., Samuel, M.S., Neumann, J., Jung, A., Huels, D., Olson, M.F., Das, S., Nibbs, R.J., Sansom, O.J., 2012. Inhibition of CXCR2 profoundly suppresses inflammation-driven and spontaneous tumorigenesis. J. Clin. Invest. 122, 3127–3144.
Kettunen, H.L., Kettunen, A.S., Rautonen, N.E., 2003. Intestinal immune responses in wild-type and Apcmin/+ mouse, a model for colon cancer. Cancer Res. 63, 5136–5142.
Kodach, L.L., Jacobs, R.J., Voorneveld, P.W., Wildenberg, M.E., Verspaget, H.W., van Wezel, T., Morreau, H., Hommes, D.W., Peppelenbosch, M.P., van Den Brink, G.R., Hardwick, J.C., 2011. Statins augment the chemosensitivity of colorectal cancer cells inducing epigenetic reprogramming and reducing colorectal cancer cell 'stemness' via the bone morphogenetic protein pathway. Gut 60, 1544–1553.
Lin, Y.C., Lin, J.H., Chou, C.W., Chang, Y.F., Yeh, S.H., Chen, C.C., 2008. Statins increase p21 through inhibition of histone deacetylase activity and release of promoter-associated HDAC1/2. Cancer Res. 68, 2375–2383.
Liu, S., Wicha, M.S., 2010. Targeting breast cancer stem cells. J. Clin. Oncol. 28, 4006–4012.
Mani, S.A., Guo, W., Liao, M.J., Eaton, E.N., Ayyanan, A., Zhou, A.Y., Brooks, M., Reinhard, F., Zhang, C.C., Shipitsin, M., Campbell, L.L., Polyak, K., Brisken, C., Yang, J., Weinberg, R.A., 2008. The epithelial-mesenchymal transition generates cells with properties of stem cells. Cell 133, 704–715.
Mantovani, A., 2009. The yin-yang of tumor-associated neutrophils. Cancer Cell 16, 173–174.
Meyerhardt, J.A., Mayer, R.J., 2005. Systemic therapy for colorectal cancer. N. Engl. J. Med. 352, 476–487.
Minder, C.M., Blaha, M.J., Horne, A., Michos, E.D., Kaul, S., Blumenthal, R.S., 2012. Evidence-based use of statins for primary prevention of cardiovascular disease. Am. J. Med. 125, 440–446.
Moser, A.R., Pitot, H.C., Dove, W.F., 1990. A dominant mutation that predisposes to multiple intestinal neoplasia in the mouse. Science 247, 322–324.
Nathan, C., 2006. Neutrophils and immunity: challenges and opportunities. Nat. Rev. Immunol. 6, 173–182.
Noy, R., Pollard, J.W., 2014. Tumor-associated macrophages: from mechanisms to therapy. Immunity 41, 49–61.
Pattabiraman, D.R., Weinberg, R.A., 2014. Tackling the cancer stem cells - what challenges do they pose? Nat. Rev. Drug Discov. 13, 497–512.
Pignalosa, D., Durante, M., 2012. Overcoming resistance of cancer stem cells. Lancet Oncol. 13, e187–e188.
Popivanova, B.K., Kostadinova, F.I., Furuichi, K., Shamekh, M.M., Kondo, T., Wada, T., Egashira, K., Mukaida, N., 2009. Blockade of a chemokine, CCL2, reduces chronic colitis-associated carcinogenesis in mice. Cancer Res. 69, 7884–7892.
Poynter, J.N., Gruber, S.B., Higgins, P.D., Almog, R., Bonner, J.D., Rennert, H.S., Low, M., Greenson, J.K., Rennert, G., 2005. Statins and the risk of colorectal cancer. N. Engl. J. Med. 352, 2184–2192.
Qian, B.Z., Pollard, J.W., 2010. Macrophage diversity enhances tumor progression and metastasis. Cell 141, 39–51.
Ridker, P.M., Cannon, C.P., Morrow, D., RIFAI, N., Rose, L.M., Mccabe, C.H., Pfeffer, M.A., Braunwald, E., 2005. C-reactive protein levels and outcomes after statin therapy. N. Engl. J. Med. 352, 20–28.
Schaefer, G., Haber, L., Crocker, L.M., Shia, S., Shao, L., Dowbenko, D., Totpal, K., Wong, A., Lee, C.V., Stawicki, S., Clark, R., Fields, C., Lewis Phillips, G.D., Prell, R.A., Danilenko, D.M., Franke, Y., Stephan, J.P., Hwang, J., Wu, Y., Bostrom, J., Sliwkowski, M.X., Fuh, G., Eigenbrot, C., 2011. A two-in-one antibody against HER3 and EGFR has superior inhibitory activity compared with monospecific antibodies. Cancer Cell 20, 472–486.
Schlossmacher, G., Stevens, A., White, A., 2011. Glucocorticoid receptor-mediated apoptosis: mechanisms of resistance in cancer cells. J. Endocrinol. 211, 17–25.
Semenza, G.L., 2003. Targeting HIF-1 for cancer therapy. Nat. Rev. Cancer 3, 721–732.
Shibata, H., Toyama, K., Shioya, H., Ito, M., Hirota, M., Hasegawa, S., Matsumoto, H., Takano, H., Akiyama, T., Toyoshima, K., Kanamaru, R., Kanegae, Y., Saito, I., Nakamura, Y., Shiba, K., Noda, T., 1997. Rapid colorectal adenoma formation initiated by conditional targeting of the Apc gene. Science 278, 120–123.
Sikandar, S., Dizon, D., Shen, X., Li, Z., Besterman, J., Lipkin, S.M., 2010. The class I HDAC inhibitor MGCD0103 induces cell cycle arrest and apoptosis in colon cancer initiating cells by upregulating Dickkopf-1 and non-canonical Wnt signaling. Oncotarget 1, 596–605.
Simon, M.S., Rosenberg, C.A., Rodabough, R.J., Greenland, P., Ockene, I., Roy, H.K., Lane, D.S., Cauley, J.A., Khandekar, J., 2012. Prospective analysis of association between use of statins or other lipid-lowering agents and colorectal cancer risk. Ann. Epidemiol. 22, 17–27.
Thurnher, M., Nussbaumer, O., Gruenbacher, G., 2012. Novel aspects of mevalonate pathway inhibitors as antitumor agents. Clin. Cancer Res. 18, 3524–3531.
Ullman, T.A., Itzkowitz, S.H., 2011. Intestinal inflammation and cancer. Gastroenterology 140, 1807–1816.
Villeneuve, P.J., Sundaresan, R.S., 2009. Surgical management of colorectal lung metastasis. Clin. Colon Rectal Surg. 22, 233–241.
Yang, P.M., Lin, Y.T., Shun, C.T., Lin, S.H., Wei, T.T., Chuang, S.H., Wu, M.S., Chen, C.C., 2013. Zebularine inhibits tumorigenesis and stemness of colorectal cancer via p53-dependent endoplasmic reticulum stress. Sci. Rep. 3, 3219.
Yuan, T.L., Cantley, L.C., 2008. PI3K pathway alterations in cancer: variations on a theme. Oncogene 27, 5497–5510.
Zhong, C., Fan, L., Yao, F., Shi, J., Fang, W., Zhao, H., 2014. HMGCR is necessary for the tumorigenecity of esophageal squamous cell carcinoma and is regulated by Myc. Tumour Biol. 35, 4123–4129.